Search for Multi-Lepton Events from Strong and Electroweak SUSY Production in pp Collisions at $\sqrt{s} = 7\,\text{TeV}$

BY PETER THOMASSEN

A thesis submitted to the

Graduate School—New Brunswick

Rutgers, The State University of New Jersey

in partial fulfillment of the requirements

for the degree of

Master of Science

Graduate Program in Physics and Astronomy

Written under the direction of

Professor Sunil Somalwar

and approved by

_____

_____

_____

New Brunswick, New Jersey

October, 2012

ABSTRACT OF THE THESIS

Search for Multi-Lepton Events from Strong and Electroweak SUSY Production in pp Collisions at $\sqrt{s} = 7\,\text{TeV}$

by Peter Thomassen

Thesis Director: Professor Sunil Somalwar

We present a search for the production of three or more isolated leptons in proton–proton collision data at $\sqrt{s} = 7\,\text{TeV}$, corresponding to an integrated luminosity of $4.98\,\text{fb}^{-1}$, that was collected by the CMS detector during the 2011 LHC run. The possible final states are classified according to a number of physical properties to properly account for varying Standard Model backgrounds and signal yields. Several supersymmetric (SUSY) models that yield multi-lepton events are investigated, and mass exclusions along with cross-section upper limits are presented for an R-parity conserving co-NLSP model, an R-parity violating model (both from strong SUSY production) as well as for several SUSY topologies that lead to electroweak pair production of charginos and neutralinos which then decay to multi-lepton final states. No new physics was observed.

Acknowledgements

First of all I would like to thank Professor Sunil Somalwar for his support and encouragement over the past months. Also, I am very thankful for every member of the High Energy Experiment group at Rutgers University whom I could work with in large-scale projects. They offered me help any time I would need it and were great company, particularly Richard C. Gray, Sanjay Arora, Emmanuel Contreras-Campana, Shruti Panwalkar, Patrick Zywicki, and Elliot Hughes. Additional thanks go to Christof Weiß for proof-reading this thesis.

The cooperation of the University of Würzburg and Rutgers brought me here and was the first step towards this project. It is kept alive by Professor Fakher Assaad and Professor Ted Williams whom I would like to thank for the opportunity to study at Rutgers. I also appreciate the financial support I received from the German Academic Exchange Service and the Foundation of German Business.

I am glad about the support and understanding my family as well as close friends and especially Caroline offered to me.

Table of Contents

List of Tables

List of Figures

Chapter 1

Introduction

Science is a phenomenon reflecting mankind's desire to understand its surroundings (and itself) in the deepest way possible while maintaining objectivity. Owing to the close connection of discovery and invention, it has led to a vast number of new technologies over the past centuries which, on the one hand, serve as tools in everyday life, and on the other hand, contribute to science's own advancement by enabling the possibilty of constructing measurement devices that are capable of measuring what is hidden from immediate perception. A very important and innovative example of this kind is the Large Hadron Collider (LHC) at CERN, Geneva (Switzerland), where the particle physics community conducts cutting-edge research experiments with the most modern technology available.

The goal of this impressive undertaking is to explore the limits of validity of the Standard Model (SM) of physics which—to our current knowledge—describes most physics of the world with unprecedented precision, and thus to probe Nature for new physics. Although this is an impressive theoretical achievement, there is reason to assume that there are physical processes that are not accounted for by the SM, not to mention gravity which the SM does not account for at all. Also, it was only recently that CERN announced with good confidence that it had succeeded observing the well-known Higgs boson [1]. This particle had been predicted by Peter Higgs as the last up-to-then unobserved elementary particle in the SM, and its existence is considered a great confirmation of the concept of the SM itself. Still, the exact properties of the Higgs boson remain unknown so far, but most of them are expected to be determined by research conducted at LHC.

Our work, however, focuses on the potential discovery of new non-SM particles

that decay preferably into at least three leptons, and on the exclusion (falsification) of certain models of interest which were devised by theorists as proposed SM extensions in order to remedy some of the issues that the SM itself leaves unanswered. In doing so, we will first give an overview of the theory of the Standard Model, emphasizing open questions and possible solutions to them (Chapter 2). Chapter 3 contains information on the structure, properties and capabilities of the Compact Muon Solenoid (CMS) detector at LHC which is used for the analysis presented in this thesis. After this general part, Chapter 4 describes the methods used in the present analysis, while Chapter 5 concludes the thesis with the analysis results.

Chapter 2

Theoretical Overview

2.1 The Standard Model

The Standard Model (SM) is a relativistic quantum field theory describing all known fundamental interactions between elementary particles with the exception of gravity, i. e. it describes electromagnetism as well as the weak and strong interactions. One has not yet succeeded integrating gravity into the same framework. However, since gravitational effects are negligible in the LHC energy range, gravity can safely be ignored for our purposes.

The SM makes use of several types of fields, each describing a different kind of particle. The model contains half-integer and integer spin particles (in units of $\hbar$) which are called fermions and bosons, respectively. The following sections are based on Refs. [2, 3] and elaborate on the individual types of particles in greater detail.

2.1.1 Fermions

The fermion group consists of two subgroups named leptons and quarks; both of them are subdivided into three so-called "generations", or "flavors".

Leptons

The three lepton generations are

$$\begin{pmatrix} \nu_e \\ e \end{pmatrix}, \quad \begin{pmatrix} \nu_\mu \\ \mu \end{pmatrix}, \quad \begin{pmatrix} \nu_\tau \\ \tau \end{pmatrix}, \tag{2.1}$$

where e, μ, τ are similar particles of electrical charge -1 and spin $1/2$. However, their masses are quite different (see Table 2.1). In interactions, they usually appear with

	particle	**mass** [MeV/c^2]	**spin**	**electrical charge** [e]
		fermions		
leptons	e	0.511	$1/2$	-1
	ν_e	$0 < m_{\nu_e} < 2.2 \cdot 10^{-6}$	$1/2$	0
	μ	105.7	$1/2$	-1
$L = 1$,	ν_μ	$0 < m_{\nu_\mu} < 0.17$	$1/2$	0
$B = 0$	τ	$1.78 \cdot 10^3$	$1/2$	-1
	ν_τ	$0 < m_{\nu_\tau} < 15.5 \cdot 10^{-6}$	$1/2$	0
quarks	u	2.4	$1/2$	$2/3$
	d	4.8	$1/2$	$-1/3$
	c	$1.27 \cdot 10^3$	$1/2$	$2/3$
$L = 0$,	s	104	$1/2$	$-1/3$
$B = 1/3$	t	$171.2 \cdot 10^3$	$1/2$	$2/3$
	b	$4.2 \cdot 10^3$	$1/2$	$-1/3$
		bosons		
$L = 0$, $B = 0$	γ	0	1	0
	g	0	1	0
	Z	$91.2 \cdot 10^3$	1	0
	$W^\pm$	$80.4 \cdot 10^3$	1	± 1
	H	$(125...127) \cdot 10^3$	0	0

Table 2.1: Elementary particles in the Standard Model [4, 5]. The Higgs boson H has not yet been observed with sufficient significance, and its precise properties remain unknown [1]. For electrically charged particles, anti-particles with opposite charge exist. Neutrinos presumably have anti-particles with opposite chirality. Anti-particles have been omitted in this summary.

the corresponding neutrino ν_i. In addition to these six particles, there are also six antiparticles with opposite charge sign and lepton number.[1] The present analysis is mainly concerned with events exhibiting three or more electrons or muons.

Quarks

There are six quarks called up, down, charm, strange, top, and bottom quark. They are organized in generations as follows:

$$\begin{pmatrix} u \\ d \end{pmatrix}, \quad \begin{pmatrix} c \\ s \end{pmatrix}, \quad \begin{pmatrix} t \\ b \end{pmatrix}, \tag{2.2}$$

where the particles in the upper row are of electrical charge $+2/3$, and those in the lower row have electrical charge $-1/3$. Anti-quarks have opposite charge and baryon number. As quarks are subject to strong interaction, they carry an additional "color" charge which is either "red", "green", or "blue".

Quarks have not been observed individually; instead, they form bound states such that the electrical charge is integer and the color charge vanishes or adds up to "white" (i. e. all three colors are present). Particles consisting of three quarks are called baryons (for example the proton: $p \mathrel{\widehat{=}} uud$), quark-antiquark combinations are called mesons (for example the pion: $\pi^+ \mathrel{\widehat{=}} u\bar{d}$).

2.1.2 Bosons

The quantum field theory on which the SM is built is invariant under Lorentz and CPT transformations, and certain gauge transformations. To prevent the theory from losing this invariance, the existence of so-called gauge bosons was predicted and observed. In addition, these particles act as the force carriers of the fundamental forces.

The most well-known one is the massless photon (γ) which is electrically neutral and mediates the electromagnetic interaction. A very similar particle, although massive, is the Z boson which can interact electromagnetically and weakly. Furthermore, the

[1] It is also possible that neutrinos are Majorana fermions and thus their own anti-particles. This question has not yet been answered experimentally.

charged W^+ and W^- bosons exist.[2] Conceptually, they have the same origin as the Z boson, which is why they take part in the same interactions. A great theoretical achievement was the unification of the electromagnetic and the weak interaction into a combined concept, the electroweak interaction.

The strong force between quarks is carried by the massless gluons (g) which come in eight different color-anticolor combinations.

2.2 Extension of the Standard Model

While the Standard Model predicts the electromagnetic, weak, and strong phenomena with extraordinary precision, there are open questions that are not addressed by the SM:

- The Standard Model does not account for *gravity* at all. It is described by General Relativity, and it is believed that, in principle, a unification of the theories is possible.
- The Standard Model contains a number of parameters that differ from expectation by several orders of magnitude for unknown reasons. For example, the mass of the Higgs boson was expected to be around 10^{15} GeV due to top quark loops, but now it appears to be on the electroweak scale, and it seems that there are delicate cancellations from other fields. This issue is referred to as the *Hierarchy Problem*.
- The Standard Model does not explain *Dark Matter*.

Several attempts have been made to find remedies for these issues from a theoretical point of view, and because they come with predictions of new particles, they are subject to experimental examination.

[2] In fact, the γ and Z fields are superpositions of the more fundamental B and W^0 fields. The B field arises from spontaneous $U(1)$ symmetry breaking, while the W^i come from the breaking of $SU(2)$.

2.2.1 Minimal Supersymmetric Standard Model

A very promising candidate for such an extension of the Standard Model is Supersymmetry (SUSY) which assigns a bosonic (fermionic) partner to every SM fermion (boson). In the superfield formalism, the minimal superpotential that can be used to construct a phenomenologically viable model with as few parameters as possible—the Minimal Supersymmetric Standard Model (MSSM)—reads

$$W_{\text{MSSM}} = \overline{u}\mathbf{y_u}QH_u - \overline{d}\mathbf{y_d}QH_d - \overline{e}\mathbf{y_e}LH_d + \mu H_u H_d. \tag{2.3}$$

Here, H_u, H_d, Q, L, $\overline{u}$, $\overline{d}$, $\overline{e}$ are the chiral superfields, and the $\mathbf{y_i}$ are 3×3 matrices acting in family space. [6]

In this scenario, the superpartners are named in close analogy to their SM partners: the fermion superpartners carry the names of their SM partners, simply preceded with an s-, while the boson superpartners have -ino appended to the SM name. In symbolic notation, sparticles are accented with a tilde. Given that the couplings, masses, and mixing angles associated with the supersymmetric fields are such that the masses of at least some of the sparticles are accessible by the LHC, it is possible to probe different variations of the MSSM at LHC.

The fact that no sparticles have been found so far implies that, for example, the selectron mass $m_{\tilde{e}}$ is much larger than the electron mass m_e. This means that, if SUSY exists, it is a broken symmetry at the electroweak scale.

Depending on the value of the coupling constants, the theory predicts different decay modes. In this search, we take an interest in decay modes that exhibit three or more leptons since such decays happen quite rarely in the Standard Model so that it should be possible to observe them at LHC, given their masses are not too high.

2.2.2 *R*-Parity

Additional terms can be added to the superpotential described in the previous section (Eq. 2.3). Doing so introduces new couplings into the model, some of which might seem contradictory to what has been observed so far. For example, there is a multiplicative

quantity called R-parity, [7]

$$R = (-1)^{3B+L+2s}, \tag{2.4}$$

where B and L are the baryon and lepton numbers, respectively, and s is the spin. As is easy to see, SM particles obey $R = +1$ so that R-parity is conserved, ensuring proton stability within the SM. Because of the fermion–boson correspondence between SM and SUSY particles, SUSY particles have $R = -1$. If one requires R-parity to be conserved, this implies that sparticles can only be produced in pairs since R-parity is a multiplicative quantity. In such models, the lightest superpartner (LSP) is stable and thus a dark matter candidate.

However, it is possible that R-partity is almost conserved, but is not exact, which still allows for a very long proton lifetime while providing a decay channel for the LSP. The corresponding extension of the superpotential reads [6, 8]:

$$W_{\text{RPV}} = \frac{1}{2}\lambda_{ijk} L^i L^j \bar{e}^k + \lambda'_{jik} L^i Q^j \bar{d}^k + \frac{1}{2}\lambda''_{ijk} \bar{u}^i \bar{d}^j \bar{d}^k + \mu'_i L^i H_u. \tag{2.5}$$

As a consequence of R-parity violation (RPV), such decays also violate lepton or baryon number conservation.

Chapter 3

Experimental Apparatus

3.1 The Large Hadron Collider

The particle collisions analyzed in the present thesis were generated by the Large Hadron Collider (LHC) which is located 100 m underground in the French–Swiss border area at the outskirts of Geneva [9]. Several pre-accelerators are employed in order to accelerate the protons to different energies and to split them into bunches, before they reach the LHC ring (see Fig. 3.1) to form two beams traveling in opposite directions. In this ring of 26.7 km circumference, 1232 superconducting dipole magnets are used to produce a magnetic field of up to 8.33 T in order to accelerate the protons to their final center of mass energy of $\sqrt{s} = 7\,\text{TeV}$.[1] Additionally, about 7000 magnets are used for trajectory corrections and bunch focusing. Once the final velocity is reached, the protons are directed onto each other on certain points around the accelerator ring, where they collide. The collision products, in general, are not stable, but decay to intermediate and final state particles which are detected by large detector devices such as ATLAS or CMS. The bunch spacing is such that interactions are separated in time by 25 ns or more to allow for more precise distinction of events.[2]

The design luminosity of LHC is $10^{34}\,\text{cm}^{-2}\text{s}^{-1}$. The instantaneous luminosity is given by

$$L = \frac{N_p^2 n_b f_{\text{rev}} \gamma_r}{4\pi \epsilon_n \beta *} F \tag{3.1}$$

[1] The maximum design energy is 14 TeV. LHC has been operating with increasing energies over the years, and it is planned to reach the design goal in 2014.

[2] However, several interactions might occur at the same time when two bunches meet. This phenomenon is referred to as "pile-up" and must be corrected for at analysis time, mostly by means of geometrical separation of the primary interaction vertex and by subtraction of expected pile-up contributions.

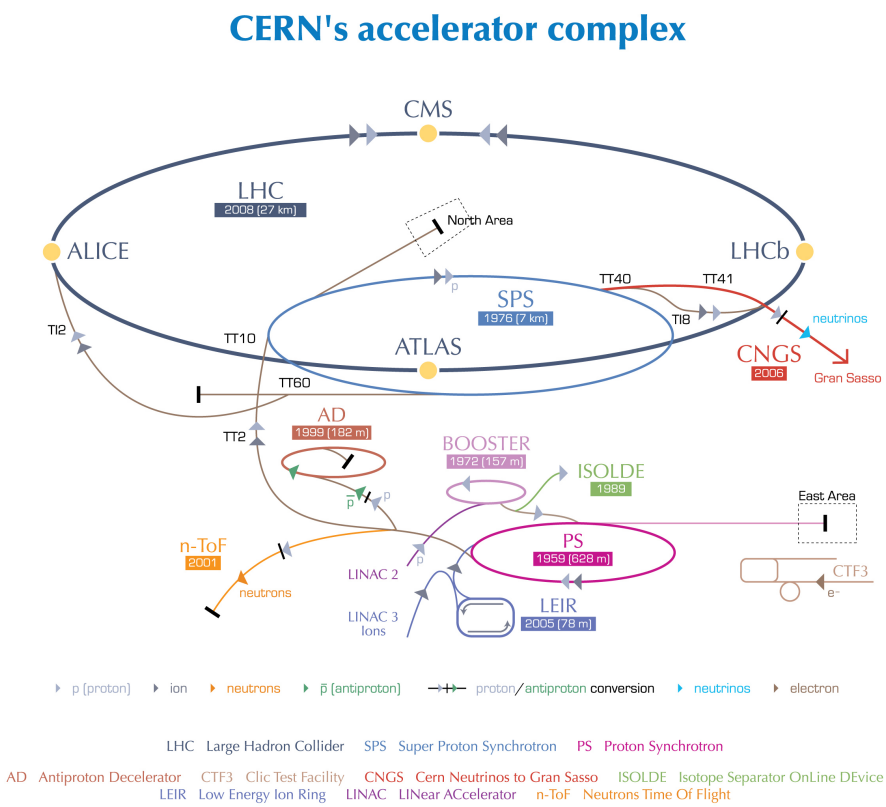

Figure 3.1: CERN Accelerator Complex [10]. The diagram shows the different accelerators, detectors, and other facilities at CERN. For proton collisions, not all of the machinery is needed: Protons are initially accelerated to 50 MeV in a Linear Accelerator (LINAC 2). Then, they are transported to the Booster (1.4 GeV), to the Proton Synchrotron (PS, 25 GeV) and the Super Proton Synchrotron (SPS, 450 GeV) from where they are injected into LHC. The PS also takes care of arranging the protons in bunches with the correct spacing for LHC.

where N_b is the number of particles per bunch, n_b is the number of bunches per beam, f_{rev} is the revolution frequency, γ_r is the relativistic gamma factor, ϵ_n is the normalized transverse beam emittance, $\beta*$ is the beta function at the collision point, and F is the geometric luminosity reduction factor due to the crossing angle at the interaction point.

3.2 The CMS Detector

The Compact Muon Solenoid (CMS) is located at point 5 of the LHC accelerator ring and one of the two large, general purpose detector systems built at LHC.[3] The CMS consists of a large superconducting solenoid which contains a silicon-based tracker,

[3]The other large detector is ATLAS, located at point 1.

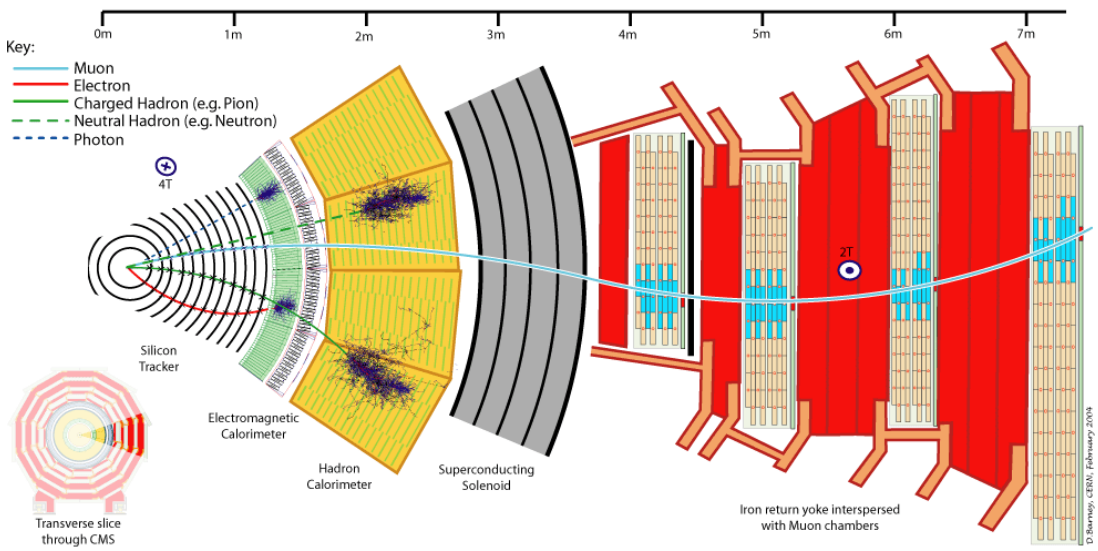

Figure 3.2: A transverse slice through CMS [11]. The illustration shows the most important detector components as well as examples of different particles as they are detected while traveling through the detector.

an electromagnetic calorimeter made of scintillating lead-tungstate crystals, and a brass-based scintillating hadron calorimeter (see Fig. 3.2); the total weight is about 12500 tons [12]. A special feature of CMS is its superconducting solenoid of 6 m internal diameter which creates a strong magnetic field (3.8 T) that is suitable for high precision measurements of charged particles at very high energies.

In order to describe the properties of particles observed in collision events, a coordinate system is used. The origin is declared where the main interaction point is expected to occur. The x axis points radially towards the center of the LHC, the y axis points in the upward direction, and together with the z axis that points along the beampipe (counterclockwise), a right-handed coordinate system is constructed. In cylindrical coordinates, the z axis is the same, ϕ is the azimuthal angle. Starting from the positive z axis, the polar angle θ increases towards the center of the LHC. Since the polar angle θ is not Lorentz-invariant, the pseudorapidity η is defined as an alternative

Lorentz-invariant coordinate,[4]

$$\eta = -\log \tan \frac{\theta}{2}. \tag{3.2}$$

When the directional separation between particles needs to be determined,

$$\Delta R = \sqrt{(\Delta\eta)^2 + (\Delta\phi)^2} \tag{3.3}$$

comes in handy as a measure of two particles' separation in η and ϕ.

After this introductory section with general information on the CMS detector, the following sections will treat the individual detector components used for the measurement of the particle properties that are recorded from collision events along the lines of Ref. [13].

3.2.1 Tracking System

In order to precisely reconstruct the path of charged particles in CMS, a tracking system based on silicon-based p–n junctions was installed. A high reverse-bias voltage is applied across the junction, creating a depletion zone with an electric field. When a charged particle passes this zone, it ionizes the silicon atoms, and the resulting electrons are free to move and create an electrical current which is detected. By setting up several layers containing a large number of such p–n junctions with small dimensions, a highly sensitive tracking device can be created. In total, 15400 tracking sensors are installed in CMS and operated at low temperature in order to minimize the effects of radiation damage. The CMS tracking system consists of several parts:

Pixel Detector

The Pixel Detector is located within 10 cm from the z axis and is used to account for small displacements close to the primary vertex, To keep the occupancy per bunch crossing reasonably low, a pixel size of 100 μm × 150 μm is used. The spatial resolution is 10 μm to 20 μm.

[4]This quantity is the massless limit of the rapidity which is an additive measure of relativistic velocity and defined as $\log \frac{E+p_z}{E-p_z}$.

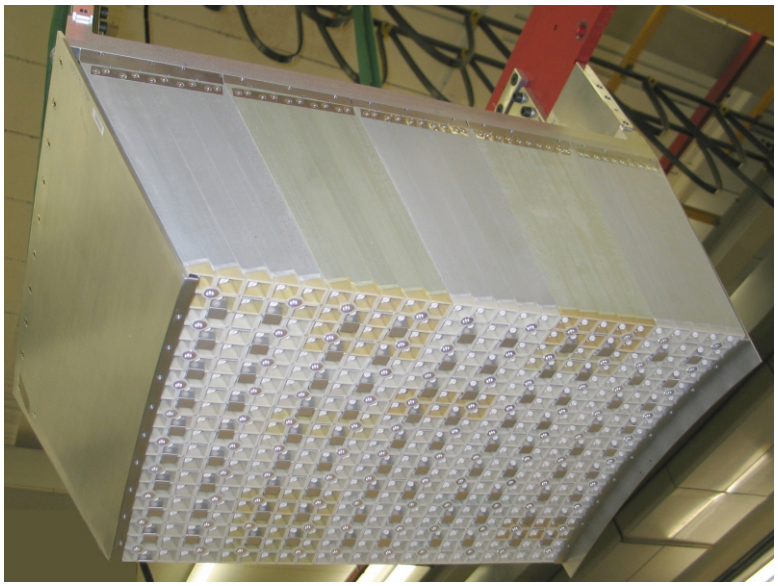

Figure 3.3: A module of the electromagnetic calorimeter consisting of 500 lead-tungstate crystals.

Strip Detector

The Strip Detectors are located in the barrel of CMS as well as in the endcap regions. In both cases, several layers of silicon strips are placed behind each other to provide similar functionality as in the case of the pixel detector. The dimensions are much wider than those of the pixels. In each detector region, they are chosen according to the corresponding production characteristics such that the occupancy will not be too high, so that a hit will provide informative value.

3.2.2 Electromagnetic and Hadronic Calorimeter

The calorimetry system is designed to measure the energies of incident particles. Depending on the particle type, the energy is deposited in different parts of the system [14]:

Electromagnetic Calorimeter (ECAL)

The task of the ECAL is to measure the energy of charged particles (especially electrons) and photons. The lead-tungstate ($PbWO_4$) material of the crystals is very dense, but optically transparent; a module is shown in Fig. 3.3. When electrons or photons travel

through, they lose energy in a cascade process due to bremsstrahlung and ionization (electrons) and e^+e^- pair production (photons). In addition, the crystals are excited so that they produce light from scintillation which can be used to infer the incident particle's energy. 80 % of the light is emitted before the next bunch crossing occurs, and is detected by photodetectors.

In the barrel ($|\eta| \leq 1.479$), there are 61200 crystals with front face dimensions of 22 mm $\times$ 22 mm, covering 0.0174 in both η and ϕ, and a length of 230 mm, corresponding to about 25 radiation lengths. In the endcap ($1.479 \leq |\eta| \leq 3.0$), there are 7324 crystals with a surface area of 28.6 mm $\times$ 28.6 mm and a length of 220 mm. An additional preshower detector is installed in front of the endcap component that helps distinguishing photons from neutral pions. This setup covers the η range up to the forward region without any gaps.

Hadronic Calorimeter (HCAL)

Like the ECAL, the HCAL is located inside the solenoid (for the most part). While the ECAL is a homogeneous, the HCAL is a sampling calorimeter which means that it consists of alternating layers of an active, signal-generating medium, and a passive medium whose only purpose is to absorb energy. The active material is a plastic scintillator which is 3.7 mm thick and organized in a tile pattern. The scintillation light emitted in a certain $\eta - \phi$ cell is summed up optically, forming a "tower", collected by wavelength-shifting fibers, and channeled to hybride photodiodes.

The barrel part ($|\eta| \leq 1.4$) has 2304 towers, each covering 0.087 in η and ϕ. There are 15 absorption layers, mostly made from brass. To increase accuracy, a number of layers is placed at the outside of the magnet coil (Hadron Outer, HO). The endcap parts cover the region $1.3 \leq |\eta| \leq 3.0$ with 19 layers of active scintillating material, covering cell of width 5° to 10° in ϕ and 0.35 to 0.09 in η. In the very forward region ($3.0 \leq |\eta| \leq 5.0$), a fourth HCAL part (Hadron Forward, HF) consisting of an active quartz fiber medium and steel absorbers is located. The quartz fiber material emits Čerenkov light that is detected by photomultipliers with resolution 0.175 in η and 10° in ϕ.

3.2.3 Muon System

The muon is about 200 times as heavy as the electron. Since the bremsstrahlung-induced dissipation in the calorimeter is proportional to mass^{-2} [15], it is suppressed by a factor of 40000. Therefore, muons can easily traverse the calorimeter system, so that other more specialized detector systems can be employed outside the calorimeter.

In the barrel, 250 drift tube (DT) chambers are used to identify muons. Four shells of stations are located at different distances from the z axis, embedded in the return yoke of the solenoid (see Fig. 3.4). In the endcap, 468 cathode strip chambers (CSC) are arranged in concentric rings, most of them containing 36 CSCs. Charged particles travelling through the gas inside a CSC cause ionization, followed by a charged avalanche whose distribution is measured on the cathode plane. From this information, it is possible to reconstruct the track geometry. Each of the DT and CSC stations is accompanied by resistive plate chambers that are used for precise timing and velocity determination.

3.2.4 Trigger and Data Storage

LHC performs about about 10^7–10^8 proton–proton collisions per second. Since not all events can be stored (about 300 Hz), a rejection rate of about 10^5 is required. First-level decisions are reached by the Level-1 (L1) trigger system which performs quick assessments of events within about 1 μs while the event data, about 0.5 MB each, is held in buffers. Potentially interesting events are then forwarded to a dedicated computing farm where high-level triggers (HLT) run more precise reconstruction algorithms in order to decide which events should be kept.

Finally, accepted events are transmitted to the storage manager system which manages the subsequent transfer to the permanent Tier-0 storage system located at the CERN main site. From there, data is distributed to interested Tier-1 and Tier-2 sites across the globe for analysis purposes. Petabyte-range storage systems are employed world-wide to manage the large amounts of data that are used on a daily basis.

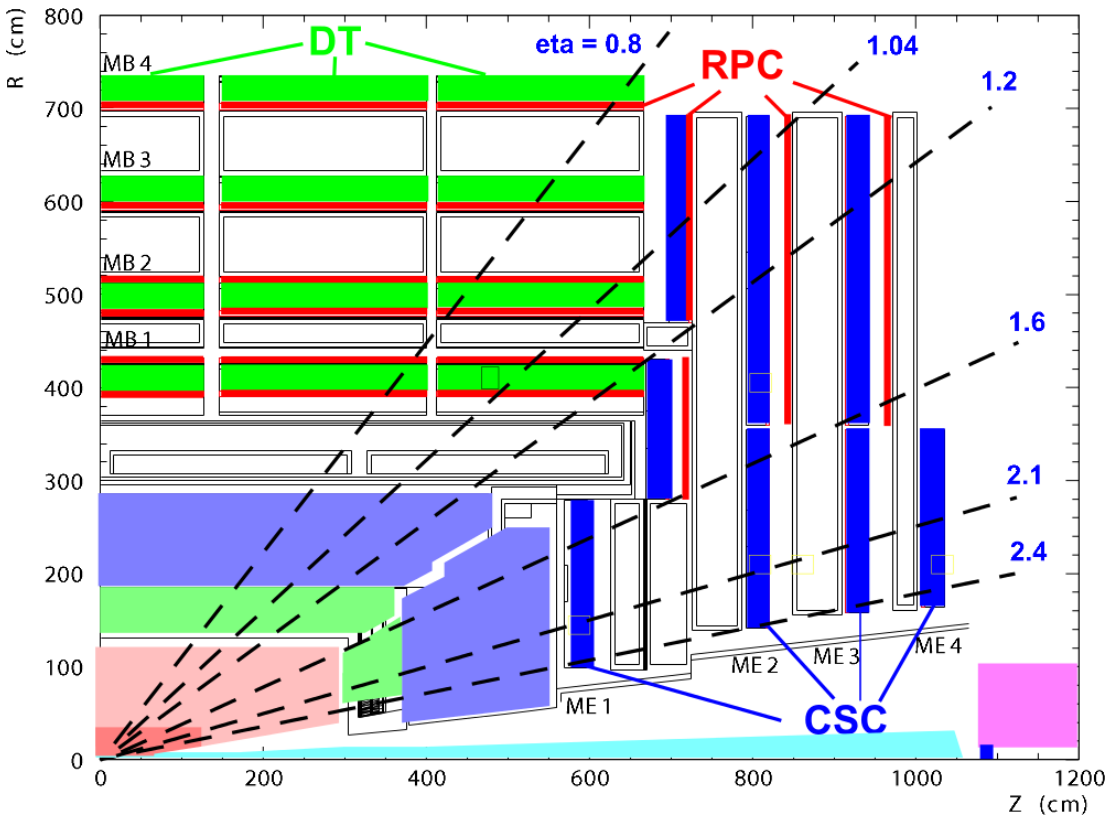

Figure 3.4: Sketch of the muon system in CMS in $r - z$ view. The drift tubes are displayed in dark-green, the cathode strip chambers in dark-blue, and the resistive plate chambers in dark-red. The light-colored areas are the tracker and calorimeter. The interaction point is located at the origin of the coordinate system.

Chapter 4

Analysis

4.1 General Approach

The goal of experimental particle physics is both the direct observation of new elementary particles that interact with the detector via the well-known interactions, and the indirect observation of new elementary particles which decay into SM particles whose anomalous production rate can be measured. At LHC, no new particles outside the SM have been observed directly so far. To observe new particles via their decays, it is required to precisely estimate the expected rate of SM events as a function of their kinematic features (like the number of leptons or the missing transverse energy $E_{\mathrm{T}}^{\mathrm{miss}}$), in order to enable the experimenter to discriminate cases of statistical fluctuations of SM processes from a significant excess in particle production that has to be judged as inconsistent with the SM. This process is called "background estimation" and is the backbone of every analysis.

Because of the discrete statistics, the kinematic properties are partitioned in bins covering a large range of the properties under consideration, and the SM background expectation is determined for each bin. While it is possible to make background predictions from data that can be validated using control samples known to be devoid of new physics, one is often forced to use Monto Carlo simulation (MC) to generate a large number of background events as prescribed by the SM. In both cases, different methods are employed.

4.1.1 Statistics

If no significant excess is observed, one can use statistical methods to examine whether the observed data can be used to falsify certain models or at least part of their parameter space. To do so, the maximal number of signal events is calculated with which the observed number of events is statistically consistent ("upper limit"). If this is less than the number of signal events expected from MC, the corresponding parameter combination is excluded.

Exclusion curves were produced at a confidence level of 95 % using the so-called CL_s technique which is explained in Refs. [16, 17].

4.1.2 Simulation

SM background MC simulations were mostly done using MadGraph [18] ($Z/\gamma*$+jets, $t\bar{t}$, di-boson), while QCD backgrounds were generated using PYTHIA 8.1 [19]. Signal simulations were done using Pythia 6.4 [8]. Detector simulation was performed using GEANT4 [20].

4.2 Multi-lepton Analysis Strategy

Focusing on events with three or more charged leptons (no more than two hadronically decaying taus), our search is designed to be very broad while avoiding any specific assumptions of new physics. The low SM background for events of this kind enables the detection of new physics with low signal yields.

Candidate events must have at least three leptons with no more than two taus, and match at least one of the following conditions:

- leading μ or e has $p_{\mathrm{T}} > 20\,\mathrm{GeV}$, and another μ or e, respectively, has $p_{\mathrm{T}} > 10\,\mathrm{GeV}$
- leading μ or e has $p_{\mathrm{T}} > 20\,\mathrm{GeV}$, and another e or μ, respectively, has $p_{\mathrm{T}} > 10\,\mathrm{GeV}$
- leading muon has $p_{\mathrm{T}} > 35\,\mathrm{GeV}$
- leading electron has $p_{\mathrm{T}} > 85\,\mathrm{GeV}$

The p_T thresholds are chosen safely above the respective trigger turn-on regime where the efficiency is maximal and has a flat shape.

By binning the data in many mutually exclusive final state bins, high sensitivity to a wide range of new physics involving leptons can be achieved [21, 22]. The variation of the background across the range of these variables determines the binning granularity: For example, the background rate depends strongly on the amount of hadronic activity H_T defined in Section 4.2.2. Thus, two H_T bins ($H_T < 200\,\text{GeV}$, $H_T > 200\,\text{GeV}$) were introduced. Similarly, the missing transverse energy E_T^{miss} (calculated as the absolute value of the p_T vectors of all particle-flow candidates [23]) was partitioned in two bins ($E_T^{miss} < 50\,\text{GeV}$, $E_T^{miss} > 50\,\text{GeV}$). Events in the high-value bins are said to satisfy the H_T or E_T^{miss} requirement, respectively.

In addition, the exclusive final states are classified by a number of criteria such as the number of leptons, the number of taus, the presence of lepton pairs consistent with a Z ("on-Z"), as well as $S_T = E_T^{miss} + H_T + \sum_{\substack{\text{isolated}\\ \text{leptons}}} |\vec{p}_T|$ which indicates the parent particle masses if most of the energy is reconstructed as E_T^{miss}, jets, or leptons. Furthermore, events are classified depending on the presence of a lepton pair with opposite-sign charge (OS), same-sign charge (SS), or same lepton flavor (SF). This allows for the separation of large backgrounds like OSSF pairs from background Drell–Yan decays. Leptons are not reused in multiple pairs: For example, $\mu^+\mu^-\mu^-$ is classified as OSSF1, $\mu^+\mu^+e^-$ as OSSF0, and $\mu^+\mu^-e^+e^-$ as OSSF2.

4.2.1 Event Trigger

The collision data used in this analysis was obtained from both single- and double-lepton triggers. The single-lepton triggers have p_T thresholds of 65 GeV for electrons and 17 GeV for muons. The double-electron trigger has 17/8 GeV, the double-muon trigger 13/8 GeV, the $e\mu$ trigger 8/17 GeV and the μe trigger 8/17 GeV, where the second number applies to the second lepton in the trigger.

In order to obtain trigger efficiencies, the H_T data sample was used. This sample is independent of the online lepton selection criteria which makes it suitable for comparison studies. The trigger efficiency is the fraction of tight leptons found in

the H_T sample for which the corresponding lepton trigger fired, and is understood as a function of p_T. For the double-electron and double-muon triggers, the asymptotic measured efficiencies are $99 \pm 4\,\%$ and $92 \pm 4\,\%$, respectively. Trigger efficiencies are used to scale the background and signal MC samples down in order to account for that fact that not all events would be caught by the trigger. The uncertainty in the trigger efficiencies translates into a systematic uncertainty for the background and signal MC.

4.2.2 Lepton Identification

Electrons and muons are reconstructed from measurements in the tracker, calorimeter, and muon system, and are required to have $p_T > 8\,\text{GeV}$ and $|\eta| < 2.1$. Candidate tracks must match with the energy deposits in the ECAL, and, for muons, with the tracks in the muon detector as described in Refs. [24, 25]. For jet reconstruction, we use the particle-flow algorithm [26] and require $|\eta| < 2.5$.

Taus decaying leptonically (τ_ℓ) are reconstructed from muons and electrons. Hadronic taus (τ_h) are reconstructed starting from a single charged track ("one-prong"). An even number of additional tracks from $\pi^+\pi^-$ pairs might be present ("three-prong", ...); however, they are not used in this analysis. In addition, the hadronic tau decay might come with a number of π^0 decays whose energy is collected in the ECAL. If there is electromagnetic energy in a cone of $\Delta R < 0.1$ around the tau candidate (as is the case for decays like $\tau^\pm \to \rho^\pm \nu_\tau \to \pi^\pm \pi^0 \nu_\tau$), we require the visible p_T of the tau candidate to be greater than $15\,\text{GeV}$, and the invariant mass of the electromagnetic energy and the track to be consistent with the visible mass expected from tau decays. If there is no electromagnetic energy in the cone (as expected for $\tau^\pm \to \pi^\pm \nu_\tau$), we require $p_T > 8\,\text{GeV}$.

The main background sources for leptons are genuine leptons inside or near jets, hadrons faking muons by punch-through into the muons system, and hadronic showers with large electromagnetic activity. Since leptons from these backgrounds occur in the vincinity of jets, they can be reduced by imposing an isolation requirement. For

electrons and muons, we define the relative isolation

$$I_{\mathrm{rel}} = \frac{\sum_{\mathrm{other}}^{\Delta R<0.3} p_{\mathrm{T}}^{\mathrm{other}}}{p_{\mathrm{T}}^{\ell}} \tag{4.1}$$

as the calorimeter energy and p_{T} sum of other tracks in the $\Delta R < 0.3$ cone around the lepton candidate divided by the lepton's p_{T}. For hadronic tau decays with electromagnetic deposit, we define the numerator of the isolation parameter I_{rel} to be the sum of the electromagnetic energy of the calorimeter towers within an annulus of $0.1 < R < 0.3$. We require $I_{\mathrm{rel}} < 0.15$ [27].

In this analysis, we are interested in "prompt" leptons originating from SUSY decays at the collision point. After applying the isolation requirement, isolated, non-prompt background leptons from heavy quark decays remain because such leptons have high p_{T} with respect to the jet axis. (If they had low p_{T}, they would not have been counted as separate leptons, but as part of the jet.) These can be eliminated by requiring that the lepton candidate be traced back to within 1 cm from the primary vertex in z, with an $x - y$ plane impact parameter d_{xy} between the event vertex and the track of $d_{xy} \leq 0.02\,\mathrm{cm}$.

Apart from ensuring the selected leptons have good quality, the lepton selection also affects the determination of the hadronic activity H_{T} which we define as the scalar sum of the transverse energies E_{T} of all jets with $E_{\mathrm{T}} > 40\,\mathrm{GeV}$ that have no selected leptons in a $\Delta R < 0.3$ cone around their axis.

4.2.3 Background Reduction

The main backgrounds for multi-lepton events with jets are $Z +$ jets, double vector boson production ($VV +$ jets), $t\bar{t}$ production, as well as multi-jet signatures from QCD. Leptons associated with jets come from heavy quark decays most of the time. By rejecting such leptons, the lepton identification requirements (isolation and vertex displacement, Section 4.2.2) reduce this background significantly. Other backgrounds such as three misidentified hadrons or cosmic rays are found to be negligible.

Further background reduction can be achieved by imposing kinematic requirements that are atypical for SM processes, as long as they are consistent with the sought-after

signal. Although, in principle, one could cut on H_{T} and $E_{\mathrm{T}}^{\mathrm{miss}}$ in order to reduce SM backgrounds, interesting signal events could become lost depending on the new physics scenario. Therefore, the different combinations of high and low H_{T} and $E_{\mathrm{T}}^{\mathrm{miss}}$ were implemented as independent channels (see previous section).

The background is further reduced by binning with respect to the "Z veto". The Z veto is declared if the selected leptons are inconsistent with lepton production from Z decays: The invariant mass of OSSF lepton pairs is required to be outside the 75...105 GeV window. A similar background contribution comes from cases where two leptons originate directly from a Z, but one of them radiates a photon which in turn produces two leptons of very asymmetric p_{T} so that one of them escapes detection. Such events are characterized by a three-lepton ($e^{\pm}e^{\mp}e$, $\mu^{\pm}\mu^{\mp}e$) invariant mass in the above window and both low $E_{\mathrm{T}}^{\mathrm{miss}}$ and H_{T}. In this case, the Z veto is also applied.

Finally, in order to reject low invariant mass Drell–Yan production of leptons as well as J/ψ and Υ meson resonances, we require the invariant mass of all OSSF lepton pairs to be greater than 12 GeV.

4.2.4 Background Estimation

Electron and Muon Backgrounds from Jets

Because of the complexity of QCD showers, the production rate of prompt, isolated electrons or muons from jets ("fake leptons") depends on factors like jet composition, jet shape, the spectrum of both the jet and the particles in it. Since these properties cannot be reliably simulated, we use data-driven methods involving jet-triggered data in order to predict the lepton fake rate for lepton-triggered samples.

More precisely, we use a jet-triggered dataset to measure a conversion factor between the rate with which jets produce isolated tracks (kaons or pions), and the rate with which jets produce isolated e/μ candidates. Using this relationship, we can predict the number of $2\ell + \ell_{\mathrm{fake}}$ events in data from $2\ell +$ tracks data. However, the conversion factor and thus the lepton fake rate depends on the fraction of heavy flavor jets in the dataset. Therefore, we consider the conversion factor as a function of $R_{d_{xy}}$, a measure

of the "flavor heaviness", which makes use of the fact that tracks from heavy flavor jets tend to have larger impact parameters. We define $R_{d_{xy}}$ as the ratio of the number of non-isolated tracks with large impact parameter ($|d_{xy}| > 0.02\,\text{cm}$) to the number of non-isolated tracks with a smaller impact parameter ($|d_{xy}| < 0.02\,\text{cm}$), and measure its value in $p_{\text{T}} = 8...24\,\text{GeV}$ for $|\eta| < 2.1$. While in datasets dominated by b-jets, the value of $R_{d_{xy}}$ is between 0.20 and 0.30, datasets with small fractions of heavy flavor jets typically have values between 0.02 and 0.03. In order to determine the number of events with fake leptons in data, the number of isolated tracks in the dataset is measured and then scaled by the conversion factor that is appropriate for the value of $R_{d_{xy}}$ as measured in the same dataset.[1] Since most events will have one fake lepton, this number is a good approximation of the number of background events.

Tau Background from Jets

Since hadronically decaying taus can only be measured using isolation requirements, fakes from jets become the most important background. In a jet dataset, all tau candidates passing the isolation cut will actually be fake taus. We define an isolation sideband ($0.20 < I_{\text{rel}} < 1.00$) and determine the conversion factor from the number of tau candidates in the sideband to the number of tau candidates that pass the isolation cut in the jet dataset. We call this factor f_t; typical values are 10 % to 20 %. If f_t was universal, it could be used directly in data to estimate the number of isolated fake taus from the number of tau candidates in the sideband.

However, isolation distributions are very sensitive to jet spectra and multiplicity, and so is f_t. To circumvent this problem, we need to find f_t as a function of another parameter that we can use as a proxy to handle these dependencies. This parameter is f_{SB}, defined as the number of non-isolated tau candidates in the sideband divided by the number of all non-isolated tau candidates. By binning the jet dataset in the p_{T} sum of all tracks, we obtain sub-datasets of different jet multiplicity and spectra. f_{SB} is very sensitive to this, and we determine the relationship between f_{SB} and f_t for each of

[1] Before scaling, the number of isolated tracks is reduced by the expected contribution from weak $t\bar{t}$ events since we use MC simulations to account for them.

these sub-datasets and store the result for later use. In general, for datasets containing mostly low p_{T} jets, f_t and f_{SB} will be larger than for datasets containing many hard jets.

Using this technique, we can determine the tau background from jets in data by binning the data in the p_{T} sum, calculating f_{SB}, and mapping it to the corresponding f_t value which we use as a conversion factor to transform the number of non-isolated tau candidates in the sideband into the number of fake taus from jets. A comparison study with jet-triggered and dilepton-triggered data shows that the $f_t - f_{SB}$ correlations hold within a systematic uncertainty of 25 %.

Irreducible Background from di-boson + jets Production

Apart from backgrounds that can be predicted using data-driven methods, there are also backgrounds that are indistinguishable from signal signatures. If one would try predicting those from data, one would end up wiping out any signal that is there. Therefore, such "irreducible" backgrounds need to be estimated from MC simulations. Instead of trusting the MC simulations, we validate them against control regions where we do not look for new physics.

Events with at least three prompt, isolated muons, with or without $E_{\mathrm{T}}^{\mathrm{miss}}$ or H_{T}, can be produced from di-boson + jets production in the SM, where WZ + jets is the dominant contribution. The bin with three leptons, $E_{\mathrm{T}}^{\mathrm{miss}}$ requirement and without Z veto is used as the control region. Comparing all allowed charge and flavor combinations ($\mu^+\mu^-\mu$, $\mu^+\mu^-e$, $e^+e^-\mu$, e^+e^-e) in this bin, it turns out that data and the MC simulation agree within the 13 % statistical uncertainty on the observation. We assign a 40 % systematic uncertainty on the fraction of WZ events where a Drell–Yan pair in the Z window was not observed to cover the $E_{\mathrm{T}}^{\mathrm{miss}}$ shape uncertainty.

The multi-lepton background from $t\bar{t}$ is estimated from MC simulations and validated in single-lepton and di-lepton control samples containing primarily $t\bar{t}$. Such a sample is obtained from single-lepton data by requiring an isolated muon with $p_{\mathrm{T}} > 30\,\mathrm{GeV}$ along with three jets, one of which must be b-tagged. In di-lepton data, we require an isolated electron and an isolated muon. A validation study shows that the number of leptons from jets and the isolation distribution are consistent with data.

Backgrounds from Asymmetric Photon Conversions

The last background, internal photon conversions, was encountered for the first time at the LHC in this analysis [28]. Such conversions happen when a final state lepton radiates a virtual photon which in turn produces an $\ell^+\ell^-$ pair. While MC generators simulate this process, they have a cut-off threshold for the conversion lepton momentum. Therefore, MC simulation does not properly account for cases where the momenta of the emitted lepton pair are very asymmetric.

Most of these cases will be caused by final state radiation from electrons that were produced in a Z boson decay. In case of an asymmetric photon conversion, the lepton with very low p_{T} can escape detection so that the invariant mass of the three remaining leptons is in the Z window.

Assuming the production rate of virtual photons leading to asymmetric conversions to be proportional to the on-shell photon production rate, we define a conversion factor (fake rate) as the probability for a photon to produce a valid lepton candidate via asymmetric conversion to the probability of the photon to be on-shell and pass all photon selection criteria, or equivalently, as the ratio of the number of $\ell^+\ell^-\ell$ events on the Z peak over the number of $\ell^+\ell^-\gamma$. Roughly, this is the share of photons producing a lepton candidate rather than being identified as a photon. Measured in a region devoid of new physics (low $E_{\mathrm{T}}^{\mathrm{miss}}$ and H_{T}), the conversion factor is determined to be $0.35\,\% \pm 0.10\,\%$ for muons and $1.1\,\% \pm 0.2\,\%$ for electrons. In addition to these statistical uncertainties, we assign a systematic uncertainty of $100\,\%$ to cover the uncertainty in the proportionality assumption.

Chapter 5

Results

5.1 Earlier Searches

Earlier searches at LHC focused on final states dominated by hadronic activity from strong production, since in general the cross-sections for such SUSY processes are considerably higher than those for electroweak production (see Fig. 5.1). As no new physics was found, squark and gluino masses were pushed up in simple SUSY scenarios by these searches. This section briefly describes two such models which would yield events with multi-lepton signatures from strong production, along with the results that were obtained from $4.98 \pm 0.11\,\mathrm{fb}^{-1}$ of data at $\sqrt{s} = 7\,\mathrm{TeV}$ acquired in the LHC 2011 run [29] using the analysis described in Chapter 4. Further information on these searches can be found in Ref. [22].

5.1.1 Slepton co-NLSP Scenario

A gauge-mediated supersymmetry breaking model with the gravitino as the lightest supersymmetric particle (LSP) was considered. Assuming a slepton to be the next-to-lightest supersymmetric particle (NLSP), there is a subtype of such models in which the right-handed sleptons are flavor-degenerate. This "co-NLSP scenario" naturally leads to multi-lepton final states via supersymmetric production through pairs of squarks and/or gluinos.

The analysis was conducted as described above. S_T bins were not useful since the LSP is stable; instead, the focus was on H_T, indicating strong production, and $E_\mathrm{T}^\mathrm{miss}$, being a sign of the LSP. No sign of new physics was found. An exclusion curve in the wino-chargino mass versus gluino mass plane for this scenario is shown in Fig. 5.2.

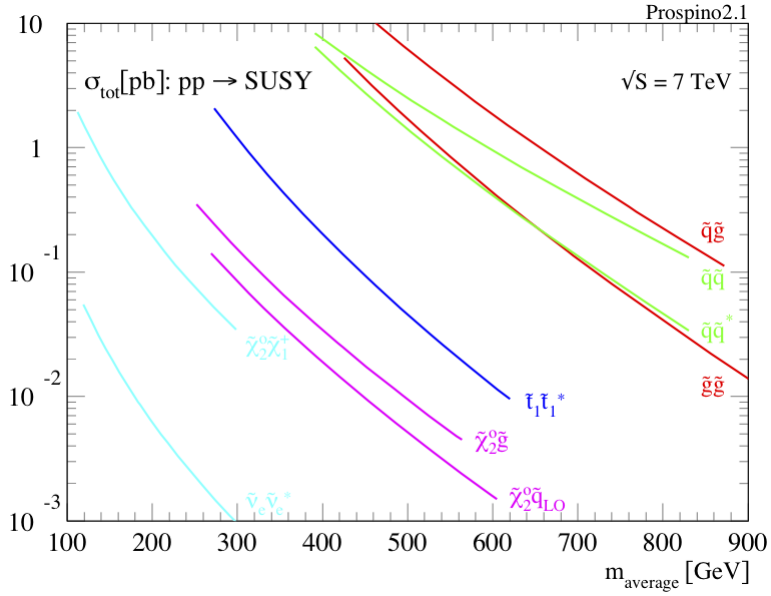

Figure 5.1: Cross-sections for $pp \rightarrow$ sparticles at 7 TeV as a function of the average sparticle mass.

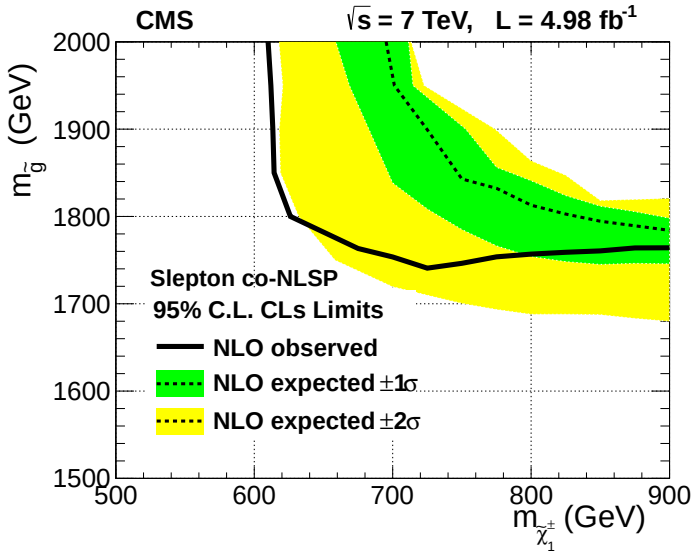

Figure 5.2: Region in the wino-chargino versus gluino mass plane that was excluded at 95 % CL in the slepton co-NLSP scenario (to the bottom-left of the black line). For comparison, the curve expected in the absence of the signal and the corresponding uncertainty bands are shown as well.

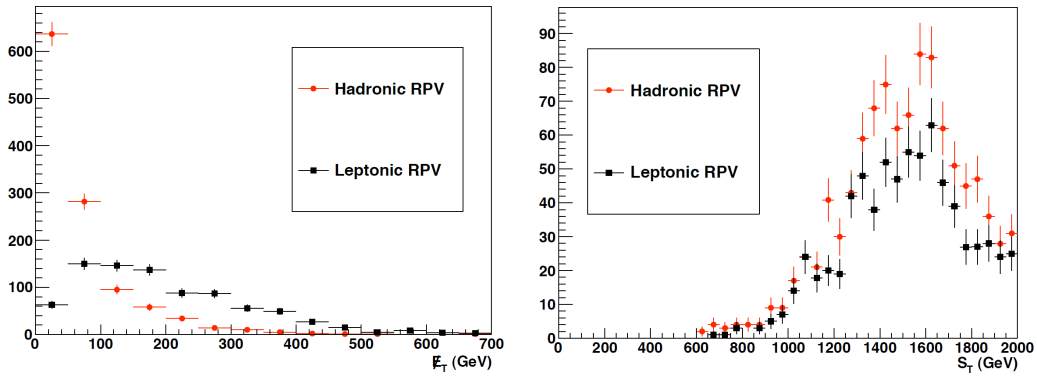

(a) Simulation of the E_T^{miss} distribution (b) Simulation of the S_T distribution

Figure 5.3: Simulations of the E_T^{miss} and S_T distribution in the RPV scenarios; y-axis in arbitrary units. [30]

5.1.2 *R*-Parity Violating Scenarios

In SUSY models where R-parity is not conserved (see Section 2.2.2), the LSP is not stable, but can decay into SM particles. Therefore, the events are not expect to show a large amount of missing transverse energy, which makes it a poor discriminator with respect to SM backgrounds (see Fig. 5.3). For this reason, S_T was used as a binning variable for RPV scenarios instead of E_T^{miss}. If most of the energy is reconstructed as E_T^{miss}, jets, or leptons, this quantity reflects the parent particle mass. For events with LSP decays, it is therefore expected to show larger values than in SM events.

Depending on the coupling vertex, leptons may arise either directly from the RPV vertex or from earlier cascade decays. Leptonic RPV with $\lambda_{e\mu\tau} = \lambda_{123} > 0.05$ and hadronic RPV with $\lambda''_{uds} = \lambda''_{112} > 0.05$ was investigated, but no signs of new physics were found for these models. Fig. 5.4 shows the excluded mass parameter region in the squark mass versus gluino mass plane for the two couplings.

5.2 Search for Direct Chargino/Neutralino Production

As discussed in the introduction to this chapter (Fig. 5.1), final states from strong SUSY production have much higher cross-sections than those from electroweak production in the same mass range. However, no sign of new physics from strong production has been observed. The absence of hadronic SUSY signals now enables the visibility of final

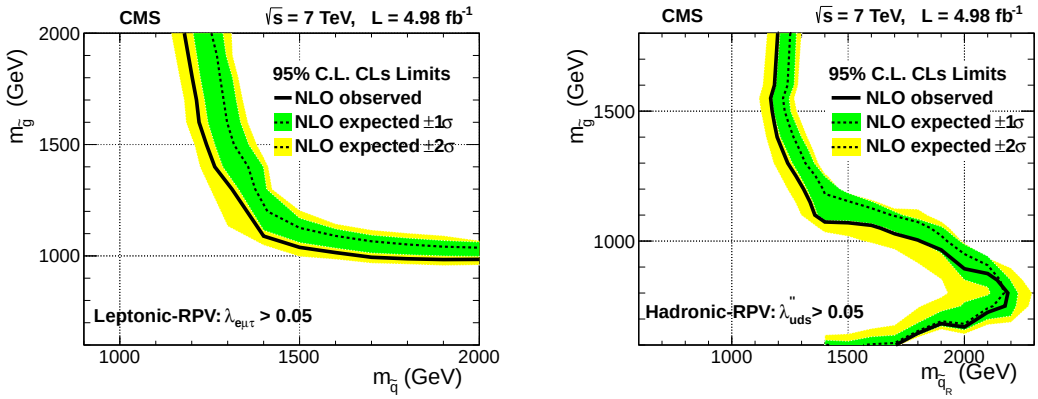

Figure 5.4: Exclusions contours in the squark mass versus gluino mass plane for the leptonic RPV scenario with $\lambda_{e\mu\tau} = \lambda_{123} > 0.05$ (left) and the hadronic RPV scenario with $\lambda''_{uds} = \lambda''_{112} > 0.05$ (right). The region to the bottom-left of the black line is excluded. For comparison, the curve expected in the absence of the signal and the corresponding uncertainty bands are shown as well.

states from electroweak production, which might have been missed in earlier searches cutting on high values of variables characterizing hadronic activity.

Final states with low hadronic activity can result from direct electroweak production of pairs of neutralinos ($\tilde{\chi}^0$) and charginos ($\tilde{\chi}^\pm$) which are mixtures of the SUSY partners of SM gauge and Higgs bosons. These sparticles may continue to decay weakly to a final state containing three charged leptons and a neutrino (see Fig. 5.5), or to a final state containing two on-shell Z or W bosons (see Fig. 5.6) [31]. Several simplified model spectra (SMS) [32] are probed. In all scenarios, the events also contain two LSPs that go undetected, leading to large $E_{\mathrm{T}}^{\mathrm{miss}}$.

We investigate two extreme cases regarding the handedness of the sleptons:

- **Left-handed sleptons:** If the sleptons are left-handed ($\tilde{\ell}_{\mathrm{L}}$), the neutralino $\tilde{\chi}^0_2$ can not only decay to a $\ell\tilde{\ell}$ pair; in fact, it decays to $\nu\tilde{\nu}$ with the same probability. Thus, in the TChiNuSlep scenarios (Fig. 5.5), two additional diagrams need to be taken into account where the $\tilde{\chi}^0_2 \to \ell\tilde{\ell} \to \ell\ell\tilde{\chi}^0_1$ leg is replaced by $\tilde{\chi}^0_2 \to \nu\tilde{\nu} \to \nu\nu\tilde{\chi}^0_1$. In this case, only 50 % of all chargino–neutralino pairs lead to three leptons.

- **Right-handed sleptons:** In the case of right-handed sleptons ($\tilde{\ell}_{\mathrm{R}}$), the chargino cannot decay weakly because the right-handed sleptons do not couple to winos [33]. Therefore, only the TChiNuSlepSlep diagram (Fig. 5.5a) contributes. The

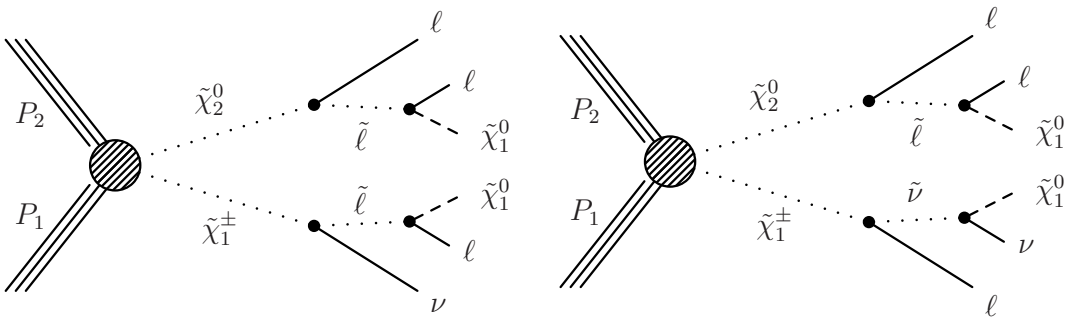

(a) TChiNuSlepSlep scenario (b) TChiNuSlepSnu scenario

Figure 5.5: Feynman diagrams for direct electroweak production of a chargino and a neutralino decaying into a final state with three leptons, one neutrino and two LSPs. Depending on the handedness of the sleptons, additional diagrams with two charged leptons replaced by neutrinos contribute, reducing the rate of three-lepton final states by 50 % (see explanation in the text).

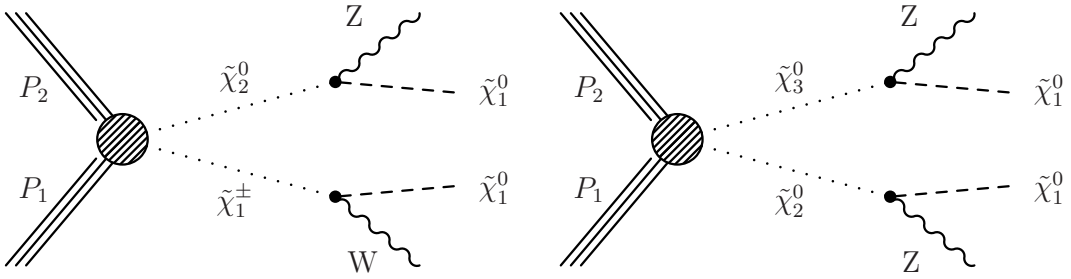

(a) TChiwz scenario (b) TChizz scenario

Figure 5.6: Feynman diagrams for direct electroweak production of a chargino and a neutralino or two neutralinos decaying into a final state with two on-shell Z or W vector bosons and two LSPs.

chargino then decays via its higgsino component in a way that is determined by other model parameters. One possibility in this context is the strongly preferred production of $\widetilde{\tau}\nu_\tau$ pairs which then result in a large amount of taus in the final state. In this case, 100 % of the chargino–neutralino pairs lead to three leptons.

Consequently, two flavor scenarios are considered:

- **Flavor-democratic scenario:** The chargino and neutralino decay weakly to the three lepton flavors with the same probability (consistent with the left-handed slepton $\widetilde{\ell}_{\mathrm{L}}$ case).
- **Tau-enriched scenario:** The neutralino decays democratically while the chargino decays to taus exclusively (consistent with the right-handed slepton $\widetilde{\ell}_{\mathrm{R}}$ case).

In the mass spectrum, the neutralino and chargino are assumed to be mass-degenerate, $m_{\widetilde{\chi}_2^0} = m_{\widetilde{\chi}_1^\pm}$, while squarks and gluinos are too heavy to be produced. In the TChiNuSlep scenario (Fig. 5.5) we consider, the slepton mass sits between the chargino–neutralino mass and the LSP mass[1], $m_{\widetilde{\ell}} = \frac{1}{2}\left(m_{\widetilde{\chi}_1^0} + m_{\widetilde{\chi}_1^\pm}\right)$. In the TChiwz and TChizz scenarios (Fig. 5.6), $m_{\widetilde{\chi}_1^\pm,\widetilde{\chi}_2^0} > m_{\widetilde{\chi}_1^0} + m_Z$, while the sleptons are assumed to be too heavy to participate.

5.2.1 Interpretation in Electroweak Scenarios

The multi-lepton analysis described in Chapter 4 was used in order to explore the electroweak SUSY processes as described in the previous section [32] based on $4.98 \pm 0.11\,\mathrm{fb}^{-1}$ of data at $\sqrt{s} = 7\,\mathrm{TeV}$ acquired in the LHC 2011 run [29]. Fig. 5.7 shows the selection efficiency (= acceptance $\times$ reconstruction efficiency) for the TChiSlepSlep topology where the chargino decays democratically. The selection efficiency vanishes if leptons with low p_{T} that espace detection are produced; this is the case if the mass difference between the LSP and the degenerate neutralino–chargino is small. With increasing mass splitting, the selection efficiency approaches 0.5.

[1] In the references, this is referred to as the $x_{\widetilde{\ell}} = 0.5$ scenario.

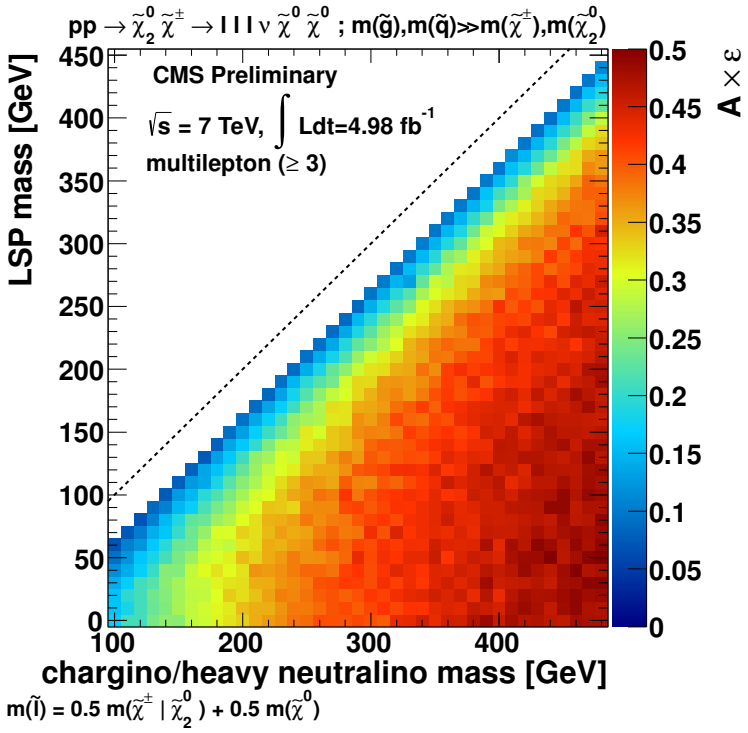

Figure 5.7: Selection efficiency (= acceptance × reconstruction efficiency) for the TChiSlepSlep topology (charginos decaying democratically). While the analysis is not very sensitive close to the diagonal (small mass splitting), good results can be expected in the other regions. [32]

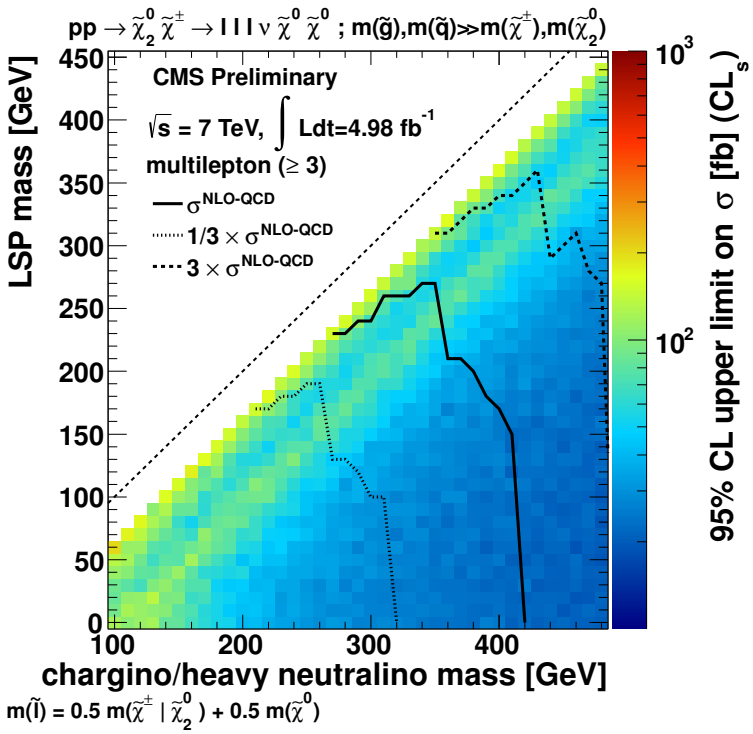

Figure 5.8: 95 % upper limit on the electroweak SUSY production cross-section (2-d color plot) in the mass plane of the LSP and the degenerate chargino/neutralino mass (TChiSlepSlep scenario). Additionally, exclusion contours are shown. [32]

The channel with the best signal-to-background ratio in this scenario is the one with three charged leptons (no taus), Z veto, and E_T^{miss} requirement. In Fig. 5.8, the 95 % upper limit on the production cross-section σ is shown the along with the expected exclusion contours. In the region where the mass splitting is close to the Z mass, the cross-section limit is less strong since sensitivity is decreased by the additional $Z \to \ell^+\ell^-$ background. Fig. 5.9 displays again the production cross-section upper limit for a massless LSP as a function of $m_{\tilde{\chi}_1^\pm,\tilde{\chi}_2^0}$.

For TChiwz and TChizz, the selection efficiency is much lower (around 0.01). Figs. 5.10 and 5.11 show the cross-section upper limits in the TChiwz and TChizz with a massless LSP, respectively, as a function of $m_{\tilde{\chi}_1^\pm,\tilde{\chi}_2^0}$. The TChizz has a stronger limit in comparison to TChiwz which is because the background for four leptons in the final state (TChizz) is considerably smaller than the background for three (TChiwz).

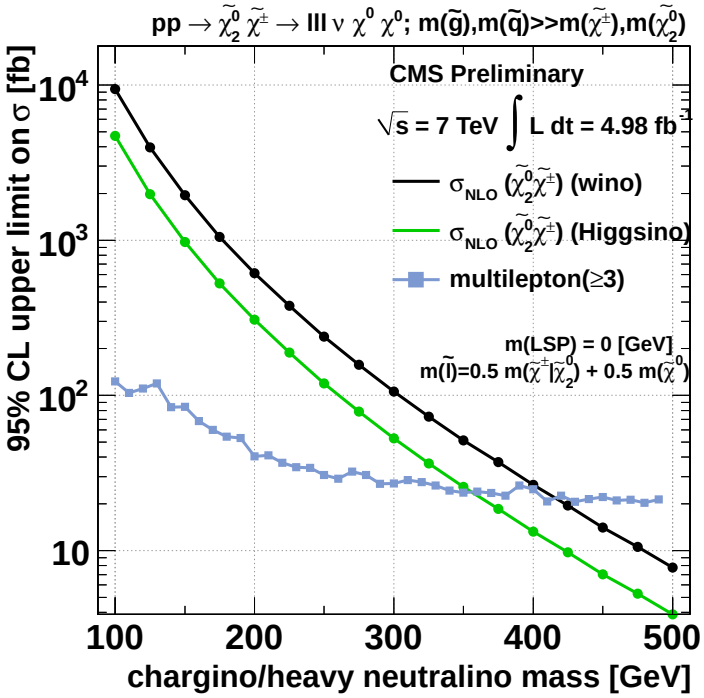

Figure 5.9: 95 % upper limit on the electroweak SUSY production cross-section for a massless LSP as a function of the degenerate chargino/neutralino mass (TChiSlepSlep scenario). [32]

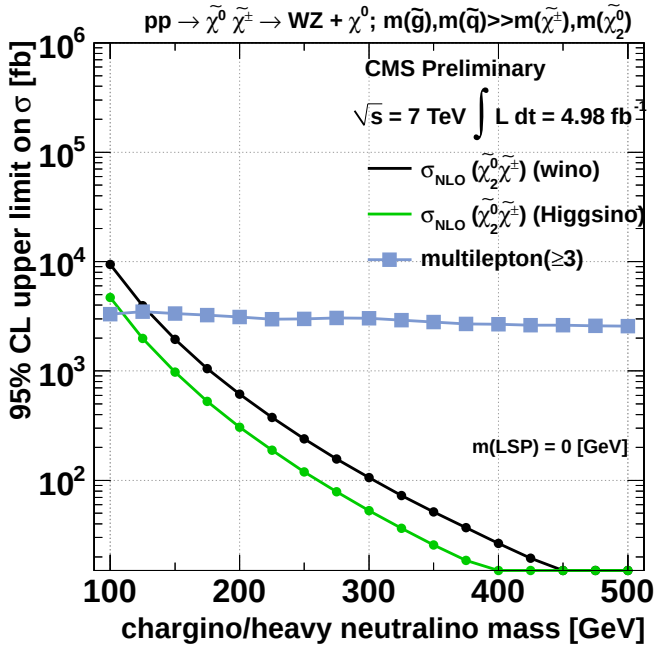

Figure 5.10: 95 % upper limit on the electroweak SUSY production cross-section for a massless LSP as a function of the degenerate chargino/neutralino mass (TChiwz scenario). [32]

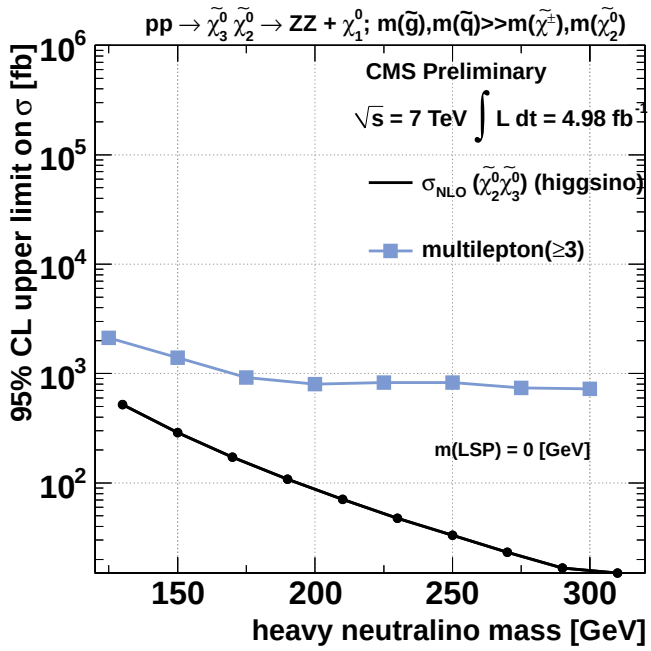

Figure 5.11: 95 % upper limit on the electroweak SUSY production cross-section for a massless LSP as a function of the degenerate chargino/neutralino mass (TChizz scenario). [32]

5.2.2 Interpretation in Electroweak Scenarios Including E_T^{miss} Shape

As explained in Section 4.2, the analysis uses two E_T^{miss} bins ($E_T^{miss} < 50$ GeV, $E_T^{miss} > 50$ GeV). The appropriate bin for this analysis is the high-valued one since missing transverse energy is expected from the neutralinos and neutrinos in the final state.

It turned out that a result that is more powerful than the one in the previous section can be obtained if the $E_T^{miss} > 50$ GeV bin is more finely split into E_T^{miss} bins of 10 GeV, since the E_T^{miss} shape in the background (see Fig. 5.12) is not the same as the signal E_T^{miss} shape in the $E_T^{miss} > 50$ GeV region. A textual representation giving a better view of the distribution tail is provided in Table 5.1.

New exclusion contours and cross-section upper limits times branching fraction for the TChiSlepSlep topology have been produced using the E_T^{miss} shape, bearing in mind the different branching fractions for the flavor-democratic and tau-enriched scenarios. The results are displayed in Figs. 5.13 and Fig. 5.14. The $m_{\tilde{\chi}_1^\pm,\tilde{\chi}_2^0}$ axis was extended in order to study the stronger exclusion.

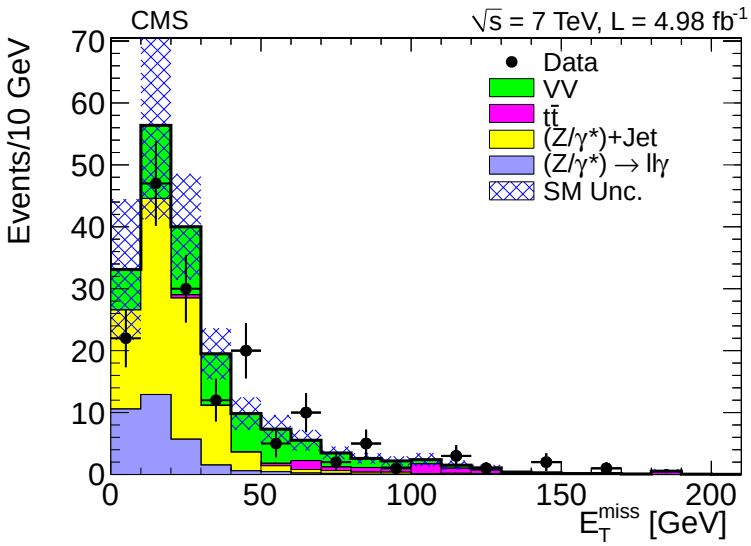

Figure 5.12: $E_{\mathrm{T}}^{\mathrm{miss}}$ distribution for the three lepton, no-Z, $H_{\mathrm{T}} < 200\,\mathrm{GeV}$ bin without taus. Comparison between the observed events and SM background is shown. The hashed bands represent the uncertainty on the background estimation. [22]

$E_{\mathrm{T}}^{\mathrm{miss}}$ [GeV]	Observation	Background
50...60	5	7.01 ± 2.15
60...70	10	5.36 ± 1.46
70...80	2	3.35 ± 0.93
80...90	5	2.52 ± 0.68
90...100	1	2.14 ± 0.56
100...110	0	2.37 ± 0.83
110...120	3	1.49 ± 0.47
120...130	1	1.06 ± 0.32
130...140	0	0.38 ± 0.11
140...150	2	0.26 ± 0.10
150...160	0	0.15 ± 0.06
160...170	1	0.16 ± 0.06
170...180	0	0.08 ± 0.03
180...190	0	0.54 ± 0.42
190...200	0	0.05 ± 0.03
> 200	0	0.33 ± 0.16

Table 5.1: Textual representation of Fig. 5.12.

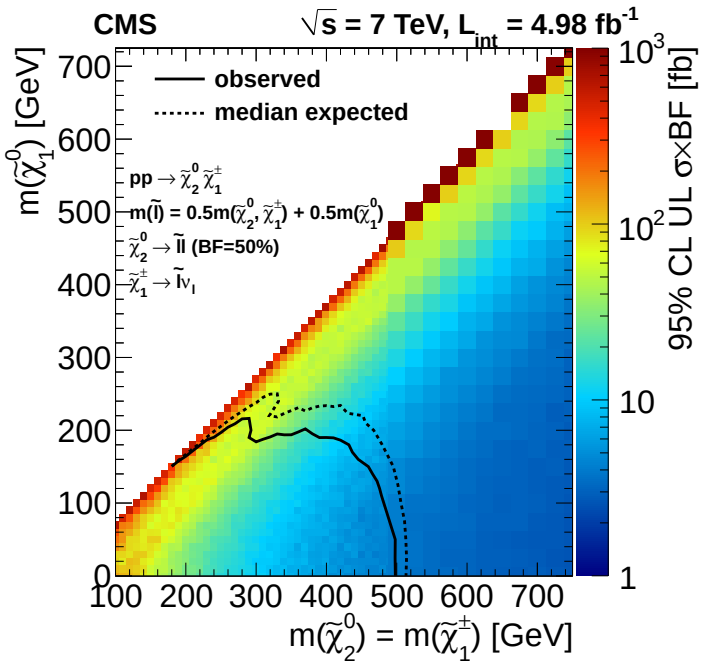

Figure 5.13: Improved 95 % upper limit on the electroweak SUSY production cross-section times branching fraction (2-d color plot) in the mass plane of the LSP and the degenerate chargino/neutralino mass using $E_{\mathrm{T}}^{\mathrm{miss}}$ shape binning (flavor-democratic TChiSlepSlep scenario). The branching fraction is 50 % as appropriate for this scenario (see explanation in the text). Additionally, exclusion contours are shown. [31]
This is an internal CMS figure and will not be made public for another month.

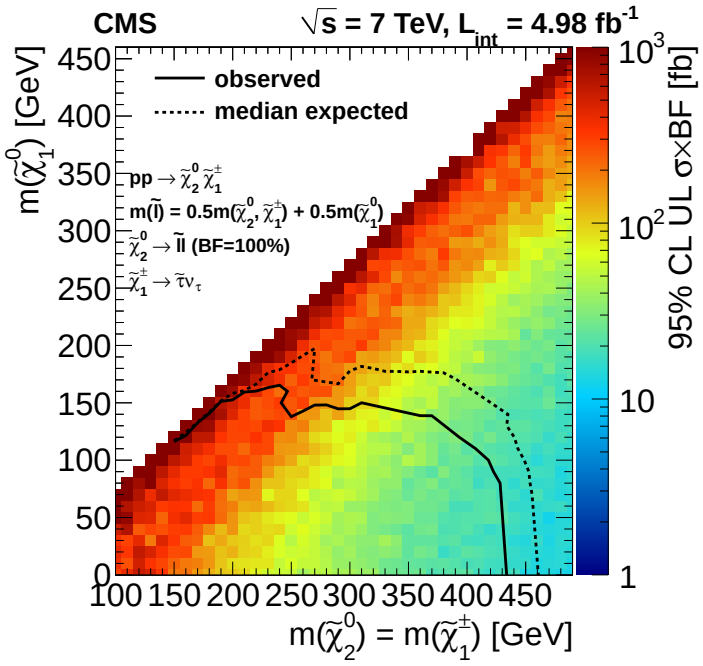

Figure 5.14: Improved 95 % upper limit on the electroweak SUSY production cross-section times branching fraction (2-d color plot) in the mass plane of the LSP and the degenerate chargino/neutralino mass using $E_{\mathrm{T}}^{\mathrm{miss}}$ shape binning (tau-enriched TChiSlepSlep scenario). Additionally, exclusion contours are shown. [31]
This is an internal CMS figure and will not be made public for another month.

5.2.3 Interpretation in Electroweak Scenarios Including $E_{\mathrm{T}}^{\mathrm{miss}}$ and M_{T}

Other studies have shown that the transverse mass M_{T} which was not incorporated in our analysis so far is also useful in the context of a search for electroweak SUSY production [31]: M_{T}, defined as

$$M_{\mathrm{T}} = \sqrt{2E_{\mathrm{T}}^{\mathrm{miss}} p_{\mathrm{T}}^{\ell} \left(1 - \cos \measuredangle(\vec{E}_{\mathrm{T}}^{\mathrm{miss}}, \vec{p}_{\mathrm{T}}^{\ell})\right)}, \tag{5.1}$$

can be used in the SM to reconstruct the mass of a W boson that decayed to a lepton and a neutrino. By the emission of leptons along with neutrinos and neutralinos in the electroweak scenarios, the shape of the M_{T} distribution is altered.

Especially in the area where the mass splitting between the LSP and the degenerate neutralino and chargino is small, taking M_{T} into account gives increased sensitivity. In order to improve our analysis results, we are planning to include this variable in our upcoming $\sqrt{s} = 8\,\mathrm{TeV}$ analysis, and use fine shape-dependent binning in the $E_{\mathrm{T}}^{\mathrm{miss}} - M_{\mathrm{T}}$ plane in order to excel the power of our previous results. In addition, we require $H_{\mathrm{T}} < 200\,\mathrm{GeV}$ and introduce b-tags in order to veto jets from bottom quarks in the electroweak search. Further information on other planned adjustments like tau identification via the HPS algorithm [34] can be found in Ref. [35].

Chapter 6

Conclusion

We have studied pp collision data at $\sqrt{s} = 7\,\text{TeV}$ collected in 2011 by CMS for an excess of events with at least three charged leptons in the final state. Both data-driven and MC simulation based background estimation techniques were used in order to discriminate Standard Model background from new physics signals; no new physics was found.

The analysis was designed to be sensitive to a wide range of new physics phenomena that will lead to multi-lepton events, and a focus was placed on both strong and electroweak SUSY production. Mass exclusion contours were presented for a slepton co-NLSP scenario as well as certain R-parity violating scenarios that produce leptons in a way that does not conserve baryon or lepton number. Both these models are based on strong production of supersymmetric particles.

Since no significant excess from such scenarios has been observed, it was possible to probe for additional models driven by electroweak production of neutralinos and charginos. We applied the analysis to different topologies, some of which produce leptons through intermediate slepton states whereas others produce on-shell Z or W bosons which subsequently decay to leptons. In doing so, we made use of the characteristic $E_{\mathrm{T}}^{\mathrm{miss}}$ shape of the signal under consideration. The result contained mass exclusion contours and cross-section upper limits.

For the future, a refined analysis is planned, involving the transverse mass M_{T} as a new variable and other improvements. The efforts are aimed to further increase the sensitivity of the analysis and push forward the cross-section limits, in order to finally uncover another piece of what Nature has not yet revealed to us.

References

[1] The CMS Collaboration, "Observation of a new boson with mass around 125 GeV", *CMS-HIG-12-028-001, in preparation*

[2] I. J. R. Aitchison, A. J. G Hey, "Gauge Theories in Particle Physics. Volume I: From Relativistic Quantum Mechanics to QED", Tayler and Francis (2003)

[3] I. J. R. Aitchison, A. J. G Hey, "Gauge Theories in Particle Physics. Volume II: Non-Abelian Gauge Theories: QCD and the Electroweak Theory", Tayler and Francis (2003)

[4] J. Beringer *et al.* (Particle Data Group), Phys. Rev. D**86**, 010001 (2012)

[5] Wikipedia contributors, "Standard Model" Wikipedia, The Free Encyclopedia, http://en.wikipedia.org/w/index.php?title=Plagiarism&oldid=5139350 (accessed July 23, 2012)

[6] S. P. Martin, "A Supersymmetry Primer" (2011), arXiv:hep-ph/9709356v6

[7] R. Barbier *et al.*, "R-parity violating supersymmetry", Phys. Rept. 420 (2005) 1, doi:10.1016/j.physrep.2005.08.006, arXiv:hep-ph/0406039v2

[8] T. Sjöstrand *et al.*, "PYTHIA 6.4 Physics and Manual" (2006), doi:10.1088/1126-6708/2006/05/026, arXiv:hep-ph/0603175v2

[9] L. Evans and P. Bryant (editors), "LHC Machine", *JINST* **3** (2008) S08001

[10] C. Lefèvre, "The CERN accelerator complex. Complexe des accélérateurs du CERN", *CERN-DI-0812015* (2008)

[11] D. Barney, "CMS Slice (2004 version)", https://cms-docdb.cern.ch/cgi-bin/PublicEPPOGDocDB/ShowDocument?docid=12

[12] The CMS Collaboration, "The CMS experiment at the CERN LHC", *JINST* **3** (2008) S08004

[13] S. Xie *et al.*, "Search for the Standard Model Higgs Boson Decaying to Two W Bosons at CMS", *CERN-THESIS-2012-068* (2012)

[14] E. Halkiadakis, "Proceedings for TASI 2009 Summer School on "Physics of the Large and the Small" : Introduction to the LHC experiments" (2010), arXiv:1004.5564v1

[15] R. K. Bock *et al.*, "The Particle Detector BriefBook", Springer (2010)

[16] T. Junk, "Confidence level computation for combining searches with small statistics", *Nucl. Instrum. Meth.* **A434** 435 (1999), doi:10.1016/S0168-9002(99)00498-2, arXiv:hep-ex/9902006v1

[17] A. L. Read, "Presentation of search results: The CL_s technique", *J. Phys. G* **28** 2693–2704 (2002), doi:10.1088/0954-3899/28/10/313

[18] F. Maltoni *et al.*, "MadEvent: Automatic event generation with MadGraph", *JHEP* **02**, 027 (2003), arXiv:hep-ph/0208156v1

[19] T. Sjöstrand *et al.*, "A brief introduction to PYTHIA 8.1", *Comput. Phys. Commun.* **178** 852–867 (2008), doi:10.1016/j.cpc.2008.01.036, arXiv:0710.3820v1

[20] S. Agostinelli *et al.*, "GEANT4: A Simulation toolkit", *Nucl. Instrum. Meth.* **A506** 250–303 (2003), doi:10.1016/S0168-9002(03)01368-8

[21] S. Arora *et al.*, "A Search for Supersymmetry with three or more leptons using 4.7 fb^{-1} of $\sqrt{s} = 7$ TeV CMS data", *CMS Analysis Note*, *CMS AN-2011/292 (v10)* (2012)

[22] The CMS Collaboration, "Search for anomalous production of multilepton events in pp collisions at $\sqrt{s} = 7$ TeV", *JHEP* **06**, 169 (2012), arXiv:1204.5341v1

[23] The CMS Collaboration, "Particle–Flow Event Reconstruction in CMS and Performance for Jets, Taus, and $E_{\mathrm{T}}^{\mathrm{miss}}$", *CMS Physics Analysis Summary*, *CMS-PAS-PFT-09-001* (2009)

[24] The CMS Collaboration, "Electron reconstruction and identification at $\sqrt{s} = 7$ TeV", *CMS Physics Analysis Summary*, *CMS-PAS-EGM-10-004* (2010)

[25] The CMS Collaboration, "Performance of muon identification in pp collisions at $\sqrt{s} = 7$ TeV", *CMS Physics Analysis Summary*, *CMS-PAS-MUO-10-002* (2010)

[26] The CMS Collaboration, "Commissioning of the particle-flow reconstruction in minimum-bias and jet events from pp collisions at 7 TeV", *CMS Physics Analysis Summary*, *CMS-PAS-PFT-10-002* (2010)

[27] S. Arora *et al.*, "Background and efficiency determination methods for multilepton analyses", *CMS Analysis Note*, *CMS AN-2011/281 (v11)* (2012)

[28] R. C. Gray *et al.*, "Backgrounds To Higgs Boson Searches from Asymmetric Internal Conversion" (2011), arXiv:1110.1368v1

[29] The CMS Collaboration, "Absolute Calibration of the Luminosity Measurement at CMS: Winter 2012 Update", *CMS Physics Analysis Summary*, *CMS-PAS-SMP-12-008* (2012)

[30] S. Arora *et al.*, "Search for Anomalous Production of Multilepton Events and *R*-Parity Violating Supersymmetry in $\sqrt{s} = 7$ TeV pp Collisions", *CMS Analysis Note*, *CMS AN-2011/174 (v21)* (2011)

[31] The CMS Collaboration, "Search for electroweak production of charginos and neutralinos using leptonic final states in pp collisions at $\sqrt{s} = 7$ TeV", *SUS-12-006*, *in preparation*

[32] The CMS Collaboration, "Interpretation of Searches for Supersymmetry with Simplified Models", *CMS Physics Analysis Summary*, *CMS-PAS-SUS-11-016* (2012)

[33] M. Chen *et al.*, "Search for Direct Electroweak Production of Charginos and Neutralinos with the Tri-lepton Plus Missing Energy Final State", *CMS Analysis Note, CMS AN-2012/059 v8* (2012)

[34] The CMS Collaboration, "Performance of τ lepton reconstruction and identification in CMS", *JINST* **7** (2012) P01001, doi:10.1088/1748-0221/7/01/P01001.

[35] S. Arora *et al.*, "A Search for Direct Chargino Neutralino production with three or more leptons using $2.5\,\mathrm{fb}^{-1}$ of $\sqrt{s} = 8\,\mathrm{TeV}$ CMS data", *CMS Analysis Note, CMS AN-2012/256 (v1)* (2012)

Vita

Peter Thomassen

Education

2011–2012 **M.S., Physics**
Rutgers University, USA (advisor: Professor Sunil Somalwar)
Thesis: "Search for Multi-Lepton Events from Strong and Electroweak SUSY Production in pp Collisions at $\sqrt{s} = 7\,\text{TeV}$"

2007–2010 **B.S., Physics**, with distinction
University of Würzburg, Germany (advisor: Professor Björn Trauzettel)
Thesis: "Entanglement of Indistinguishable Particles: Application to Carbon Nanotube Quantum Dots"

Experience

2011– **Research Assistant**, Rutgers, The State University of New Jersey, USA
CMS Experiment at the CERN Large Hadron Collider

Publications

CMS Collaboration, "Search for anomalous production of multilepton events in pp collisions at $\sqrt{s} = 7\,\text{TeV}$", *JHEP* **06**, 169 (2012), arXiv:1204.5341v1

Hall-Wilton, R. et al., "Studies of PLT-type single-crystal diamond pixel detectors", *NSS/MIC, 2011 IEEE*, pp.1150–1155, 23–29 Oct. 2011 (2011)

CMS Public Documents

CMS Collaboration, "Searches for Supersymmetry using Multilepton Signatures in pp Collisions at 7 TeV", *CMS Physics Analysis Summary*, CMS-PAS-SUS-11-013, (2011)

CMS Internal Documents

S. Arora et al., "A Search for Direct Chargino Neutralino production with three or more leptons using 2.5 fb^{-1} of $\sqrt{s} = 8\,\text{TeV}$ CMS data", *CMS Analysis Note*, CMS AN-2012/256 (2012)

S. Arora et al., "A Search for Supersymmetry with three or more leptons using 4.7 fb^{-1} of $\sqrt{s} = 7\,\text{TeV}$ CMS data", *CMS Analysis Note*, CMS AN-2011/292 (2011)

S. Arora et al., "Search for Anomalous Production of Multilepton Events and R-Parity Violating Supersymmetry in $\sqrt{s} = 7$ TeV pp Collisions", *CMS Analysis Note*, CMS AN-2011/174 (2011)